Euler/Lagrange Computations of Sprays Produced by Different Liquids Using a Generalised Stochastic Droplet Collision Model

M. Sommerfeld*[1], M. Sui[1], S. Lain[2]
[1]Multiphase Flow Systems, Otto-von-Guericke-University Magdeburg
Hoher Weg 7b, D-06130 Halle (Saale), Germany
[2]Department of Energetics and Mechanics, Universidad Autónoma de Occidente
Cali, Colombia
*Corresponding author email: martin.sommerfeld@ovgu.de

Abstract
Recent experimental data on binary droplet collision outcomes in the form of collision maps allow the extension and further validation of the previously proposed boundary line models. This concerns the lower bouncing boundary, the boundary between both stretching as well as reflexive separation and the coalescence region. All the proposed boundary lines include the effect of droplet size ratio. The bouncing boundary based on Estrade et al. (1999) was extended to include dissipation effects and the dependence of the two involved parameters on the non-dimensional impact parameter B. The stretching separation boundary was based on combining correlations proposed by Jiang et al. (1992) and Brazier-Smith et al. (1972) for including droplet size ratio and dissipation effects. Unfortunately, not for all experimental cases on equal sized binary droplet collisions the proposed boundary lines yield a perfect agreement. In order to demonstrate the effect of such differences (modelled boundary lines and experimentally observed boundary lines) in the presumed droplet collision maps, numerical spray simulations were conducted using the Euler/Lagrange approach with the fully stochastic droplet collision model as recently presented by Lain and Sommerfeld (2020). For that purpose, a relative dilute reference spray is considered where the spray properties at a injection plane are obtained from experiments.

Keywords
Turbulent sprays, Euler/Lagrange approach, stochastic collision model, droplet collision maps, boundary line models.

Introduction

Although turbulent sprays have been numerically computed for many years on the basis of the parcel-based Euler/Lagrange approach (Dukowicz, 1980; O`Rourke, 1982), a reliable prediction is not yet possible as an accurate and generalised droplet collision model is still missing. In the past several such models were developed and applied, but they very often have the problem of being strongly dependent on grid resolution and number of tracked parcels (see for example Zhang et al. 2012). With respect to detecting possible collisions between a tracked parcel and millions of surrounding parcels, one may distinguish between deterministic and stochastic approaches to find such an occurrence (see Sommerfeld 2017). Most accurate are of course deterministic tracking models which however are very time consuming since the two parcels with crossing trajectories have to be found. On the other hand, stochastic collision models are very efficient, but the result may be affected by the statistical evaluation of the collision probability. The most common model, namely the semi-stochastic collision detection model of O`Rourke (1981) is based on first determining the possibility of a collision between two droplet parcels residing in the same control volume. Hence this approach is deterministic in that sense that possible collision pairs are searched among the real parcels, however only within a certain neighbourhood. Then a stochastic

process is applied in order to decide whether a collision is occurring based on the kinetic theory collision probability. Hence, the collision detection is not based on parcel tracking up to the collision as done in a fully deterministic model. The largest problem of this model is the dependence of the collision rate on the imposed search volume, which is in the classical model the local computational cell. These issues were for example analysed in detail by Pischke et al. (2015) comparing the results for different approaches for collision detection. The very recent study of Lain and Sommerfeld (2020) showed that the fully stochastic collision model (see also Rüger et al., 2000) is very insensitive with respect to grid size, tracking time step and considered number of tracked parcels.

A very important issue in determining whether two droplets moving on a collision trajectory eventually really collide is the so-called "impact efficiency" which accounts for the phenomenon that small droplets might move around the larger collector droplet with the relative flow (see for details Ho and Sommerfeld, 2002; Sommerfeld and Lain, 2009; Sommerfeld and Lain, 2017). The analysis of Lain and Sommerfeld (2020) has shown that this effect in a spray, with normally wide size distributions, results effectively in a reduction of the collision rate by 20%. Hence neglecting this phenomenon yields in an overprediction of droplet size due to too many coalescence events. Surprisingly this effect, although remarkably reducing the effective collision rate, has been until today not considered in spray combustion simulations (see e.g. Perini and Reitz, 2016).

Finally, the collision model needs to properly determine the collision outcome which may be bouncing, coalescence or separation. This decision is based on so-called collision maps (i.e. the non-dimensional impact parameter B (i.e. $B = 2\,b/(d_S + d_L)$ with b the droplet lateral displacement and d_S *and* d_L *the* diameters of small and large droplets) versus the collision Weber (i.e. $We = \left(\rho\ d_S\ u_{rel}^2\right)/\sigma$)) number whose structure unfortunately strongly depends on the kind of liquid considered (demonstrated by: Sommerfeld and Kuschel (2016); Finotello et al. (2018a); Sommerfeld and Pasternak (2019); Al-Dirawi and Bayly (2019)). More generalised collision maps were recently developed by Sommerfeld and Pasternak (2019) for the coalescence boundaries and by Sui et al. (2019) for the bouncing boundary. This article summarises the present status by also considering recent experiments which allow an extension of the suggested modelling approach.

Generalised Collision Maps

The droplet collision map (i.e. B = f(We)) is a well-established approach for deciding on the outcomes of binary droplet collisions, which may be bouncing, coalescence and reflexive as well as stretching separation observed in the lower Weber-number regimen (e.g. We < 200). These collision maps are indispensable for numerical simulations of spraying systems. Unfortunately, such nomograms are not unique and depend on the physical properties of the system (i.e. surrounding gas and droplet liquid) as well as the kinematics of the collision. Naturally, the non-dimensional impact parameter B and the We-number do not consider all these properties. This would imply a new measurement whenever a new droplet liquid is considered. This of course we anticipate to avoid; the model should be predictive.

For separating the different collision outcome scenarios, normally theoretically based boundary lines are being used. However, also these mostly do not include all relevant properties and need to be first validated. Therefore, the attempt in this study is to extend existing correlations for bouncing (Sui et al. 2019), to introduce dependences for the triple point location (Sommerfeld and Kuschel 2016) and use correlations for the critical Weber-number location (Sommerfeld and Pasternak 2019). Whenever new experimental data with

new substances are available, these allow extension or confirmation of the introduced approach and correlations.

In this section such recent developments in the establishment of generalised droplet collision outcome maps will be summarised. The boundary line between reflexive separation and coalescence (RS-C) could be successfully described by the correlation of Ashgriz and Poo (1990), however, shifted by the critical Weber number We_C. So far viscous dissipation was not included in this consideration. This modified correlation accounts for the effect of droplet size ratio and is given by:

$$We_{RS-C} = \left(We_C - We_{C,w}\right) + 3\left[7\,(1+\Delta^3)^{2/3} - 4(1+\Delta^2)\right]\frac{\Delta\left(1+\Delta^3\right)^2}{\Delta^6\,\eta_S+\eta_L} \quad (1)$$

where $We_{C,w}$ is the critical Weber number for the reference liquid pure water. The critical Weber number for any liquid considered so far was found to be well represented by the correlation of Qian and Law (1997), as confirmed also by Sommerfeld and Pasternak (2019):

$$We_C = \sqrt{2}\,480\,\mathrm{Oh} + 15 \quad (2)$$

with the Ohnesorge number (i.e. $Oh = \mu/\sqrt{\rho\ \sigma\ d_S}$) characterising the type of liquid and considering the small droplet diameter. The new data for the critical We-number from Pan et al. (2016) for water, water/Glycerol (30%) mixtures and Ethanol follow this trend line quite well. The results for the HPMC (hydroxypropyl methylcellulose) solution in water (Al-Dirawi and Bayly 2019) showed for the concentrations of 2 and 4% a critical Weber-number in the measurement range below We = 100 which were only located slightly above the correlation (Eq. 2). Hence this equation seems to be supported by experimental data at least until $Oh < 0.1$ as commented by Sommerfeld and Pasternak (2019).

The location of the boundary line between stretching separation and coalescence (SS-C) was so far quite well described by the combination of the two boundary lines of Jiang et al. (1992) and Brazier-Smith et al. (1972):

$$B = \frac{C_a}{1.14\cdot We^{1/2}}\left[1+\frac{\mu}{\sigma}\left(\frac{\rho\,d_s}{\sigma}\right)^{1/2}\right]\cdot\left[\left(\frac{1}{\Delta}\right)^3 - 2.4\left(\frac{1}{\Delta}\right)^2 + 2.7\,\frac{1}{\Delta}\right]^{1/2} \quad (3)$$

Here the first bracket term accounts for the influence of fluid properties and the second term respects the influence of size ratio. It was demonstrated by Sommerfeld and Pasternak (2019) that this approach is applicable for a size range of $0.5 < \Delta < 1.0$. For smaller size ratios the Brazier-Smith et al. (1972) correlation yields a too strong shift of the boundary line to the right-hand side to larger We and upwards to higher B. Additional, theoretical analysis is necessary to solve this issue. As demonstrated by Lain and Sommerfeld (2020) the droplet collision size ratio in a typical spray may have values between 0.1 and 0.3.

The key idea of this model was using the triple point as a reference location which was very well correlated with the Capillary number ($Ca = Oh\,\sqrt{We} = f(Oh)$) for many types of liquids, including pure fluids and solutions (Sommerfeld and Kuschel 2016). A triple point location (i.e. coincidence of bouncing, stretching separation and coalescence) could be also identified from the recent measurements of (Al-Dirawi and Bayly 2019) for HPMC solutions as well as Pan et al. (2016) for water, Glycerol/water mixtures and Ethanol. Besides these pure liquids also the influence of surfactants on binary droplet collisions was studied and a number of droplet collision regime maps were presented. Actually, a surfactant admixture completely modified the collision maps for the same liquid; especially the bouncing regime was drastically enlarged. This is of course associated with the drastic reduction of surface tension due to the surfactants. For the pure liquid the triple point location matched with the correlation given below (Equation 4), but for the surfactant solutions the triple point data did not match the proposed correlation.

Therefore, special types of liquids including surfactants are not covered by the proposed model and will need different theoretical approaches and additional experimental studies.

$$We_T = (-0.0088/Oh + 5.4246 - 2.2036\ Oh)^2 \quad (4)$$

By enforcing now the Jiang et al. (1992) boundary line (see Eq. 3) to go through this triple point with the knowledge of We_T and B_T one may obtain the values for the constant C_a (please note that the constant C_b in the original formulation was assumed to be unity):

$$C_a = B_T\, We_T^{\frac{1}{2}} \left[1 + \frac{\mu}{\sigma}\left(\frac{\rho\, d_S}{\sigma}\right)^{0.5}\right]^{-1} \quad (5)$$

The results for this constant including the old data (Sommerfeld and Pasternak 2019) and some recent measurements are shown in Figure 1 for pure fluids and solutions, respectively. The new data clearly confirm the appropriate choice of the correlations and the differences between pure fluid and solutions regarding the choice of the constant C_a:

$$C_a = 2.3 - 11.12 \cdot Oh + 23.74 \cdot Oh^2 - 18.2 \cdot Oh^3 \quad \text{Pure fluids} \quad (6)$$

$$C_a = 2.63 - 7.2 \cdot Oh + 7.86 \cdot Oh^2 + 1.4 \cdot Oh^3 \quad \text{Solutions} \quad (7)$$

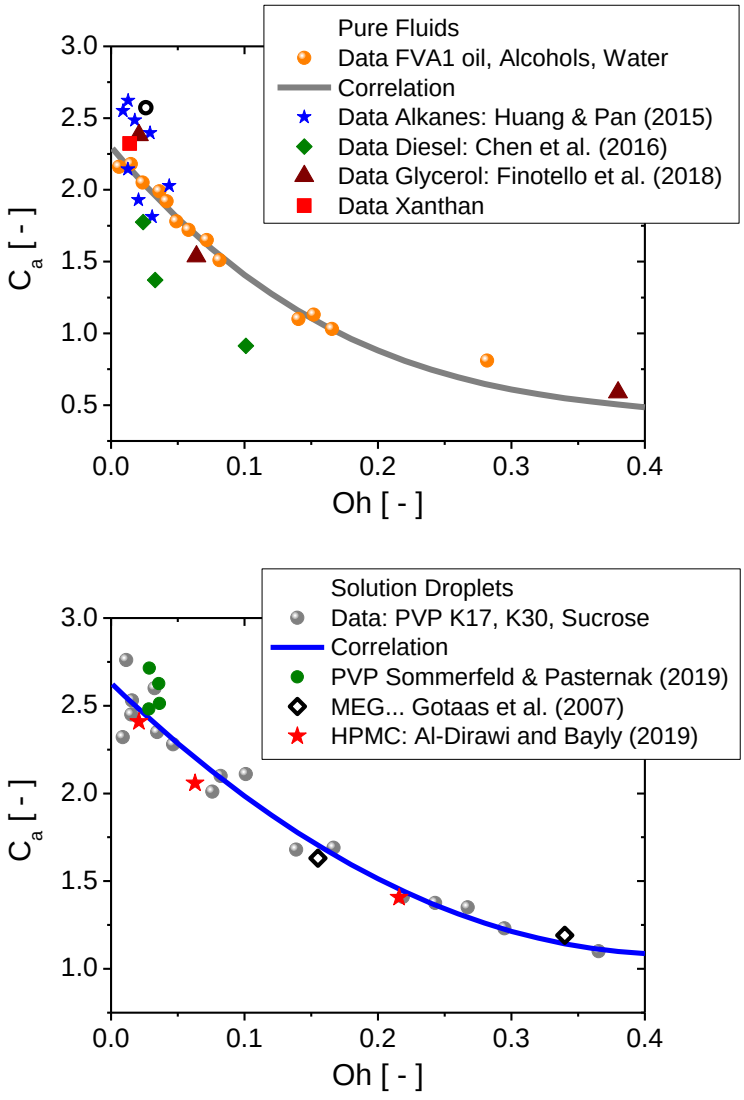

Figure 1: Comparison of the experimental data for C_a in the boundary line model of Jiang et al. (1997) as given by Eqn. (3) and (5) between stretching separation and coalescence for pure fluid droplets (a) and solution droplets (b) with the proposed third order polynomials given by Eqn. (6) and (7) (Assumption: C_b = 1.0).

The new experimental data for a mixture of water and glycerol (Finotello et al. 2018a)) and Xanthan (Finotello et al. 2018b)) follow closely the proposed correlation. The same applies for a series of measurements conducted for different alkanes, however using two droplet sizes, namely 300 and 600 μm (Huang and Pan 2015). Concerning the data for Diesel (Chen et al. 2016) only the first point matches quite well, whereas the other two are a bit below the correlation. These results actually stem from mixtures of regular Diesel with Biodiesel (which is supposed to be ethanol) which are normally fully miscible although there are appreciable differences in dynamic viscosity and density. May be a new correlation would yield a slight upward shift of the curve to a value of around 2.5 at the abscissa and thereby better match with the solution results. For solution droplets recently measurements with HPMC (hydroxypropyl methylcellulose) were conducted by Al-Dirawi and Bayly (2019) for three concentrations. The resulting data for C_a nicely follow the proposed correlations. Also, the recent measurements with low-viscosity PVP (polyvinylpyrrolidone) are very close to the original proposal (Figure 1 b)). With the resulting SS-C boundary line, a satisfactory representation for a number of pure liquids and solutions was possible (Sommerfeld and Pasternak 2019).

So far, the lower bouncing boundary was mostly represented by the correlation presented by Estrade et al. (1999) and adapted to other liquids through a modification of the shape factor (see Sommerfeld and Kuschel 2016). Actually, this shape factor describes the deformation of the droplets during the collision process and it should therefore be dependent on the type of liquid (i.e. viscosity and surface tension) and in addition the impact parameter B. The major problem with this model is however that any dissipation effects were neglected in the derivation. The original correlation for the lower bouncing boundary is (Estrade et al. 1999):

$$We = \frac{\Delta\,(1+\Delta^2)\,(4\,\phi_0 - 12)}{\chi\;(1-B^2)} \tag{8}$$

$$\chi = 1 - 0.25\,(2-\tau)^2(1+\tau) \quad if: \tau > 1$$

$$\chi = 0.25\,\tau^2\,(3-\tau) \quad if: \tau \le 1$$

$$\tau = (1-B)\,(1-\Delta)$$

where χ is the ratio of interaction region volume of the larger droplet to the total volume of both droplets.

Based on numerical simulations with interface reconstruction (i.e. VOF, volume of fluid method) Hu et al. (2017) introduced a dissipation term in the energy balance which resulted in an additional parameter in the boundary line equation, valid for equal sized droplets:

$$We = \frac{(1+\Delta^3)\,(1+\Delta^2)\,(4\,\phi_1 - 12)}{(1-\alpha_1)\;(1-B^2)\,\Delta^2} \tag{9}$$

Since they only considered liquid aluminium droplets, a fixed set of parameters was specified, i.e. $\alpha_1 = 0.5$ and $\phi_1 = 4.25$. Based on these studies Al-Dirawi and Bayly (2019) proposed a bouncing model also including a dissipation parameter estimated from their experiments with HDMC solutions and a variable shape factor derived for an oblate spheroidal droplet at B = 0. Hence, the bouncing boundary was specified as:

$$We = \frac{12\,\Delta^2\,(1-\Delta^3)\,(1+\Delta^2)\,(\phi_2 - 1)}{(\chi_S + \Delta^3\,\chi_L)\,(1-\alpha_2)\;(1-B^2)\,\Delta^2} \tag{10}$$

Here χ_S and χ_L characterise again the volumes of the interaction region for small and large droplets and ϕ_2 is the new shape factor only dependent on size ratio and other fitting parameters which have been adapted for the considered fluids, similar to the dissipation parameter α_2 (Al-Dirawi and Bayly 2019).

In this study we have chosen a slightly different approach which allows an automated adaptation of the bouncing boundary according to the liquid considered and also accounts for the effect of B (i.e. lateral collision) on the shape parameter as well as an energy conversion rate parameter β (Sui et al. 2019). Performing again an energy balance with dissipation, the bouncing boundary has of course the same form as that derived by Hu et al. (2017):

$$We = \frac{(1+\Delta^3)(1+\Delta^2)(4\phi - 12)}{(1-\beta)(1-B^2)\Delta^2} \tag{11}$$

As one would expect, the maximum deformation with a complete transformation of kinetic energy into surface energy and dissipation is found for a head-on collision with B = 0. For any larger impact parameters B, the droplet deformation and hence also dissipation is smaller. Therefore, as a first step a linear relation between shape and conversion factor and the impact parameter is assumed:

shape parameter: $$\phi(B) = -k_\phi(Oh)\cdot B + \phi_{init}(Oh) \tag{12}$$

energy conversion parameter: $$\beta(B) = k_\beta(Oh)\cdot B + \beta_{init}(Oh) \tag{13}$$

In order to account for the fluid properties, it should be tried to establish the four parameters in these equations (Eqn. 12 and 13) to be dependent on the Ohnesorge number. The remaining task is to determine the slopes and the intercepts of both parameters $\phi(B)$ and $\beta(B)$. This is done on the basis of numerous experimental data initially for the collision of identical sized droplets carrying identical liquid. For that purpose, the boundary line according to Eq. (11) was fitted to the experiments and adapted by variation of the parameters (Eqn. 12 and 13). Here it should be noted that ϕ_{ini} mainly determines the crossing point with the horizontal axis We_{B-C} and k_ϕ roughly the limiting B-value at larger We. By this try-and-error procedure the data points presented in Figure 2 for the four model parameters in Eqn. (12) and (13) could be determined. Regarding the shape parameter $\phi(B)$ it was found that the data are best represented by third order polynomials which show different behaviour for pure fluids and solutions. The fitting parameters for solution droplets are for the range of Ohnesorge numbers considered always below those for pure fluids. This should be caused by different deformation behaviour of these two kinds of fluids.

$$\begin{cases} k_{\phi,fluid} = -9.6\,Oh^3 + 10.93\,Oh^2 - 4.03\,Oh + 0.82 \\ \phi_{init,fluid} = -11.7\,Oh^3 + 12.4\,Oh^2 - 4.32\,Oh + 3.9 \end{cases} \tag{14}$$

$$\begin{cases} k_{\phi,solution} = -87.7\,Oh^3 + 52.5\,Oh^2 - 10.2\,Oh + 0.725 \\ \phi_{init,solution} = -18.25\,Oh^3 + 18.31\,Oh^2 - 6.05\,Oh + 3.76 \end{cases} \tag{15}$$

Most of these correlations fit the experimental data quite well which all are decreasing continuously with growing Oh-number approaching some limiting value. For fluid droplets experimental data expand up to Oh < 0.5 and for solution droplets until Oh < 0.4. In some cases, a limiting value for the parameter has been specified such as: $\phi_{init,fluid} = 3.4$ for $Oh > 0.4$; $k_{\phi,solution} = 0.0834$ for $Oh > 0.2$ and $\phi_{init,solution} = 3.1$ for $Oh > 0.4$. The experimental data considered in this study were only those presenting full collision maps including of course all boundaries and especially the lower boundary of bouncing. These data are:

For pure fluids: alcohols and refence oils (Sommerfeld and Kuschel 2016), different alkanes including tetradecane (Qian and Law 1997, Huang and Pan 2015) and Diesel-Biodiesel mixtures Chen et al. (2016) and mixture of water and glycerol (Finotello et al. 2018a).

For solution droplets: PVP (polyvinylpyrrolidone) polymer solutions with different solids content and sucrose solutions (Kuschel and Sommerfeld 2013) as well as HDMC (hydroxypropyl methylcellulose) solutions with different solids content (Al-Dirawi and Bayly 2019).

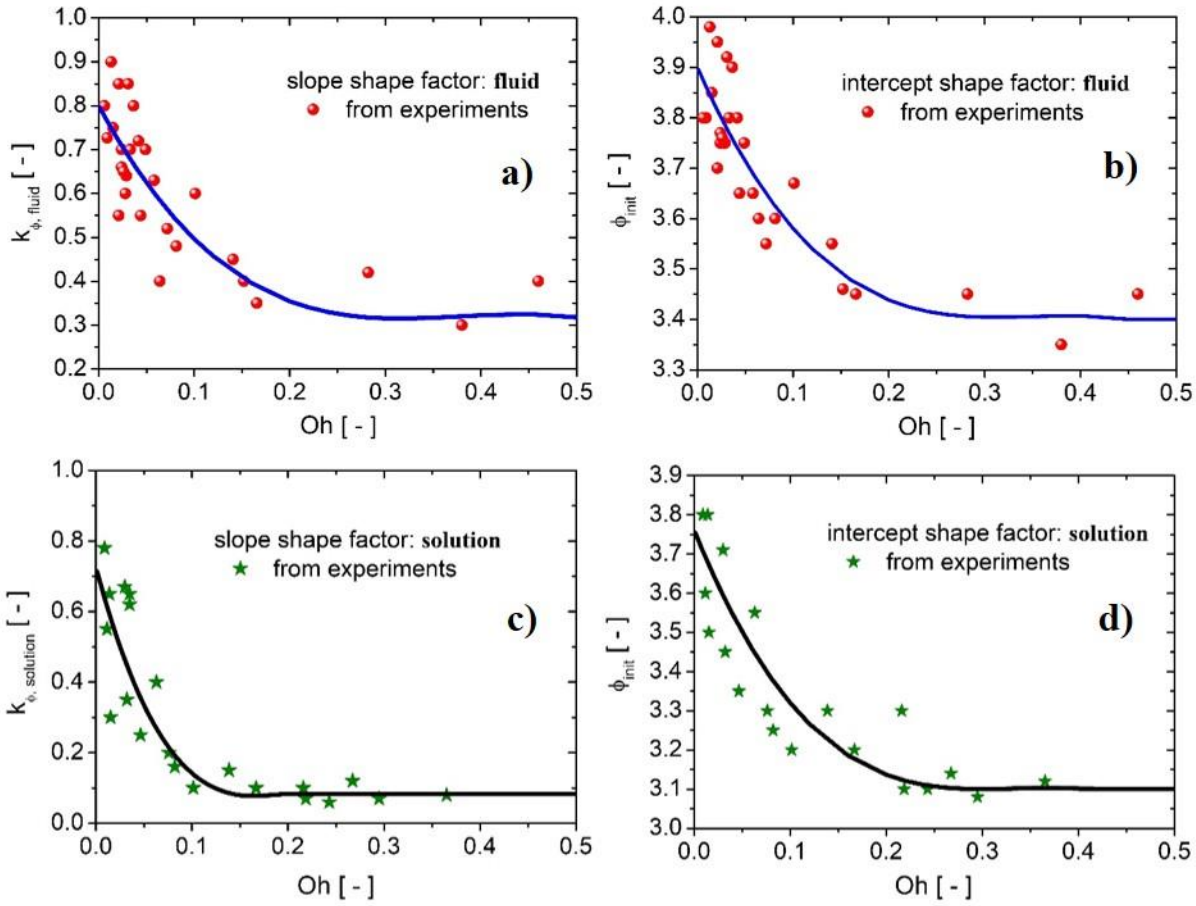

Figure 2: Experimental data points for the parameters of the shape factor ϕ in Eq. (13), namely the slope values ($(a)\ k_{\phi,fluid}$ and $(c)\ k_{\phi,solution}$) and the interception values ($(c)\ \phi_{init,fluid}$ and $(d)\ \phi_{init,solution}$) for pure fluid as well as solution droplets together with the proposed polynomial correlations (Eqn. (14) and (15)).

On the other hand, it was found that the energy conversion parameter β showed no distinct differences for both kinds of fluids, indicating the same behaviour regarding the energy dissipation. The two parameters in Eq. (13) are again represented by the following polynomial fittings considering all experimental data listed above:

$$\begin{cases} k_\beta = 1 - \beta_{init} \\ \beta_{init} = 22.6\,Oh^3 - 19.6\,Oh^2 + 5.24\,Oh + 0.07 \end{cases} \tag{16}$$

The values for β_{init} rise continuously with growing Ohnesorge number and approach a limiting value of $\beta_{init} = 0.5$ for $Oh > 0.15$.

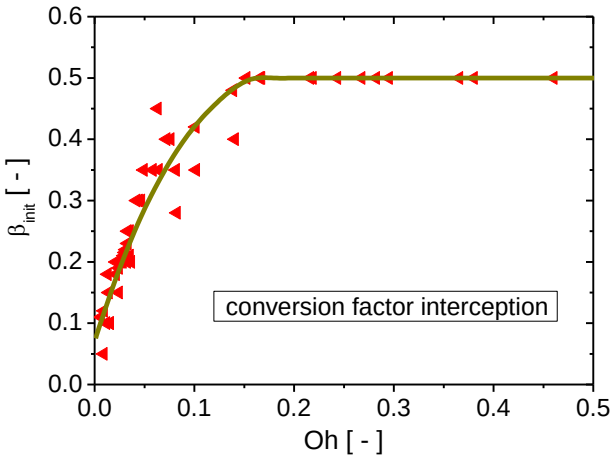

Figure 3: Experimental data points for the parameters of the conversion factor β in Eqn. (13), namely the interception values β_{init} in dependence of Ohnesorge number together with the proposed third-order polynomial fitting (Eq. (16)).

Composite Droplet Collision Model

With the new model for the bouncing boundary and the further validation of the other models, i.e. RS-C and SS-C, the generalisation of the droplet collision outcome maps is further improved. In the following, recent measurements as summarised above for different kinds of liquids, will be used for validation, namely pure fluids and solutions. For most of the liquids considered, a region of bouncing is observed for large impact parameters B over the entire low Weber (We) number regime (i.e. let's say below We ≈ 150) and for low We numbers over the entire B regime (see Sommerfeld and Pasternak, 2019). Moreover, due to interfacial effects and the special composition of milk, no bouncing was observed at all (Finotello et al. 2018a)). All other liquids seem to have collision maps with the same fundamental outcome regimes were bouncing additionally covers the low We regime over 0 < B < 1. However, the location of the boundary lines is strongly depending on the type of liquid considered and hence mainly the viscosity, as well as the size ratio of colliding droplets, which however will not be further analysed here. In the following some experimental collisions maps together with the proposed boundary lines will be presented in order to demonstrate the feasibility of the composite model.

In Figure 4 the new boundary models are compared with the experiments of Finotello et al. (2018a) for Glycerol at different concentrations and hence dynamic viscosity. The mixture of Glycerol/water is treated as a fluid. For the lower Glycerol concentrations, the agreement is almost perfect regarding all boundary lines. The region of reflexive separation is moving to the right just like in the experiments whereby the coalescence domain is growing. For the highest Glycerol concentration (see Figure 5) there are some differences between model and experiment. First of all, the SS-C boundary is slightly below the experiments, which is caused by the experimental triple point lying slightly above the proposed correlation (Equation 5). Also, the lower bouncing boundary is predicted to be shifted to higher Weber numbers so that the bouncing domain is overpredicted. Therefore, also tuned boundary lines are included which fit the experimental data much better. This tuning was done by just modifying the parameters in the bouncing boundary and the SS-C boundary by try and error in order to establish a better agreement with the measurements. Inasmuch such a shifted collision map will influence the collision rates in a spray, and the predicted Sauter mean diameter will be analysed below.

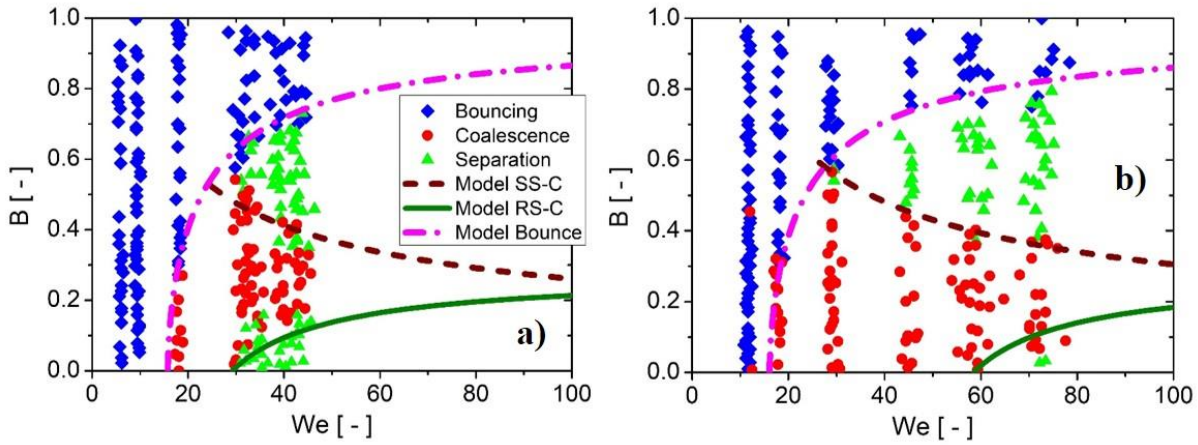

Figure 4: Experimental binary droplet collision maps for **water-Glycerol mixtures** {**(a)** 40 %, Oh = 0.021; **b)** 60 %, Oh = 0.064} from Finotello et al. (2018a) together with the proposed boundary line models for bouncing, SS-C and RS-C.

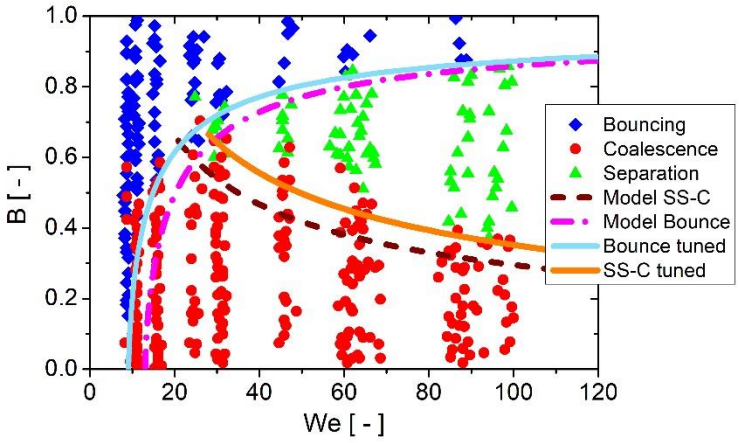

Figure 5: Experimental binary droplet collision map for **water-Glycerol (**80 %, Oh = 0.381) mixtures with from Finotello et al. (2018a) together with the proposed boundary line models for bouncing, SS-C and RS-C and tuned boundary lines to match the experiments.

The comparison for milk concentrates, being a quite complex liquid, as discussed by Finotello et al. (2018a) is presented in Figure 6 for two contents of dry substance (TS). As mentioned before, no bouncing region was observed in the experiments. Unfortunately, such a phenomenon needs to be known in advance when anticipating numerical spray simulations and developing an appropriate collision map for describing droplet collision outcomes. Milk powder dissolved in water is of course a solution including many different components. Nevertheless, both SS-C boundary lines are included in Figure 6, for a pure liquid as well as for a solution in order to highlight the differences to be expected. The solution boundary line is very close to the experiments, but with a slight upward offset. The complementary fluid SS-C boundary is well below the experimental boundary region for both TS-cases (Figure 6 a) and b)). The boundary line for RS-C very well captures the experimental data for both TS. Unfortunately, the solution SS-C boundary according to the model does not very well fit the experiments for the very high solids content (46 % TS) and is actually completely off. This might be associated with a possible non-Newtonian behaviour of the liquid, but also come from inhomogeneities with the colliding droplets.

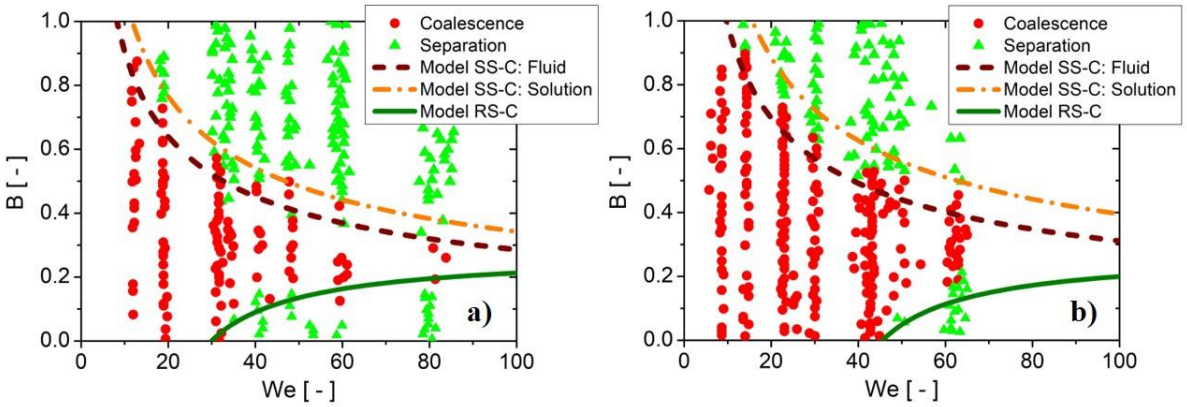

Figure 6: Experimental binary droplet collision maps for **water-milk powder solution** with different dry substance (TS) {**a)** 20 % TS content, Oh = 0.022; **b)** 30 % TS content, Oh = 0.050} from Finotello et al. (2018a) together with the proposed boundary line models for SS-C and RS-C.

The binary collision behaviour of droplets carrying a non-Newtonian liquid (namely a 500 ppm xanthan solution) was also analysed by Finotello et al. (2018b) with the same experimental setup. With this liquid three known collision outcome scenarios were observed, namely bouncing, stretching separation and coalescence (see Figure 7). Surprisingly for this case both the proposed bouncing and SS-C boundaries very well capture the experimental observation.

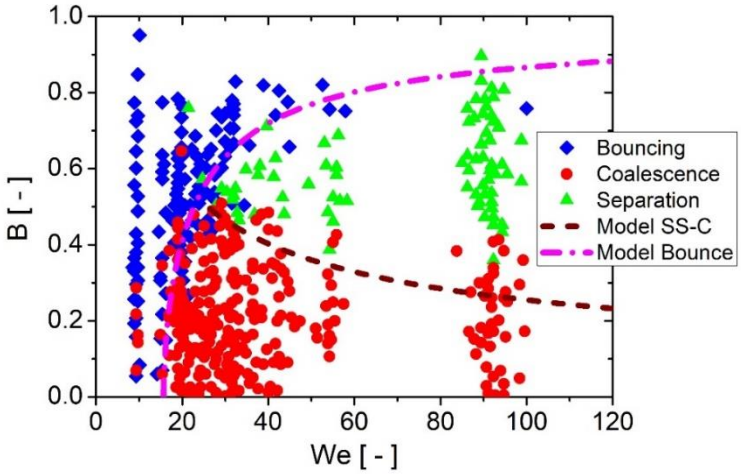

Figure 7: Experimental binary droplet collision maps for a **500 ppm xanthan solution** (Oh = 0.014) from Finotello et al. (2018b) together with the proposed boundary line models for bouncing and SS-C.

Still diesel is an important fuel which is injected into the combustion chamber by high pressure nozzles. Naturally collisions between droplets are important and should be modelled properly. Previously already the SS-C and RS-C boundary could be matched (Sommerfeld and Pasternak 2019). Now the new bouncing model is shown also in Figure 8, matching almost perfectly with the experiments (Chen and Chen 2006) for the size ratio $\Delta = 1$. The proposed bouncing boundary includes of course the size ratio (see Equation 11) which however needs to be validated using additional measurements.

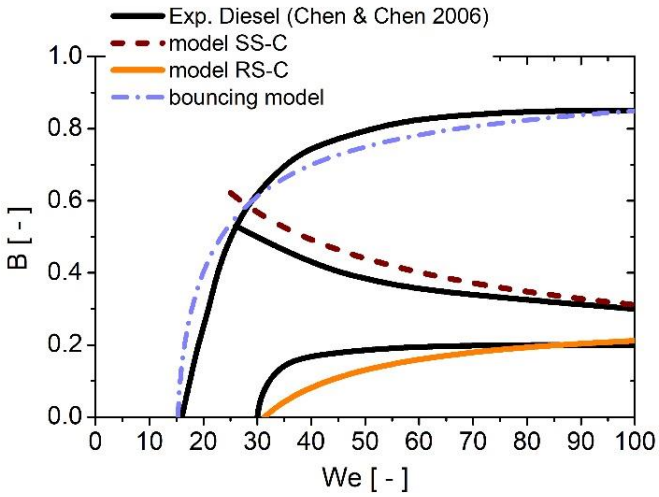

Figure 8: Comparison of experimental Diesel droplet collision map (see Chen and Chen 2006) with the proposed boundary lines for bouncing and separation (i.e. SS-C and RS-C).

Spray simulation results

For conducting an analysis of the applied droplet collision models including the proposed collision outcome maps, the Euler/Lagrange parcel approach was applied to a selected reference spray (details in: Rüger et al. 2000). This spray is relatively dilute, but still remarkably affected by droplet collisions, and was initiated by injecting measured droplet size and velocity characteristics over the inlet plane as described by Lain and Sommerfeld (2020). This approach does not require the consideration of a droplet breakup model. The performance of the spray computations and the stochastic droplet collision model with regard to grid cell dimensions and parcel number was evaluated considering the development of the averaged Sauter mean diameter along the spray and local droplet size distributions. Moreover, the influence of the predefined collision map structure on the predicted spray properties was studied in detail by Lain and Sommerfeld (2020).

Here the numerical spray simulations shall be used to quantify the difference in the predicted spray properties for cases where the proposed model predicts a different droplet collision outcome as observed experimentally. As an example, the water-Glycerol 80% is selected where both the SS-C and the bouncing boundary line are not predicted perfectly by the model (see Figure 5). Thereby eventually the uncertainties to be expected when applying the present modelling approach may be quantified.

The Euler/Lagrange approach applied here with the k-ε turbulence model, two-way coupling and all models considered for droplet parcel tracking have been described previously by Lain and Sommerfeld (2020). Here the same computational domain and standard grid resolution is used. Moreover, turbulent droplet dispersion and the full droplet collision model is applied. In the previous part only results with a size ratio of one $\Delta = 1$ were considered wherefore in the numerical simulations the boundary lines shown in Figure 5 were considered to be fixed with $\Delta = 1$. The following correlations are considered for the **model case**: SS-C boundary Equation (2) combining the Jiang et al. (1992) and the Brazier-Smith et al. (1972) approach and bouncing by Equation (11). For the **tuned case,** the included parameters were varied in such a way to yield good agreement with the measurements (see Figure 5). Comparing the two simulations is done by considering the conditional numbers of droplet collisions along the spray as shown in Figure 9. For the considered spray the collision Weber number is relatively

low so that bouncing is the dominating collision outcome. As to be expected from Figure 5, using the model boundary lines regardless of experimental agreement yields an overprediction of bouncing and consequently a remarkable reduction of coalescence. On the other hand, the size of the stretching separation region is only slightly modified giving initially almost identical collision outcomes for both assumptions. Only further downstream the assumed model (Figure 5) causes an overprediction of stretching separation.

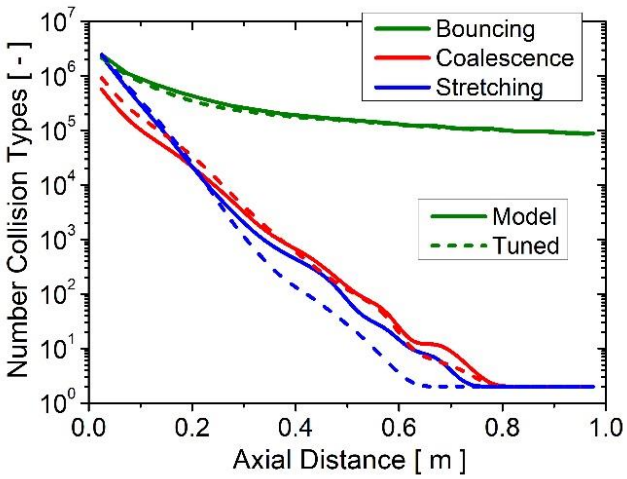

Figure 9: Conditional number of droplet collisions along the spray (i.e. bouncing, coalescence and stretching separation for the slightly incorrect model compared to the tuned boundary correlation which better match the experiments (water-Glycerol, 80 %, Oh = 0.381).

It has been previously demonstrated that the droplet velocity profiles throughout the spray are hardly affected by the choice of the droplet collision outcome map (Lain and Sommerfeld 202). As a result of the decreasing number of coalescence events for the modelled collision map compared the experimental one the Sauter diameter along the spray is underpredicted, however only by about 1 %.

Conclusions

Recent studies on the development of generalised binary droplet collision models are introduced where the collision outcome maps with appropriate boundary lines between the regimes are used. The lower bouncing boundary including dissipation effects was developed considering a large number of new experimental data. For the demarking the stretching separation and coalescence regimes a combination of the Jiang et al. (1992) and the Brazier-Smith et al. (1972) approach was found to be useful for droplet size ratios $\Delta > 0.5$. The collision maps of a number of different liquids may be well fitted, however further examinations are required especially with respect to the colliding droplet size ratio. With the help of numerical spray simulations by the Euler/Lagrange approach with the fully stochastic collision model it was possible to quantify the resulting errors in case the boundary lines of the proposed composite model do not properly fit to the experimental collision map. If this difference is not too large, e.g. $\pm$ 5% in the impact parameter and about 10% in the Weber number, also the predicted droplet velocities and sizes do not deviate too much from the experimental observation.

Acknowledgments

The second author acknowledges the financial support of this research project by the China Scholarship Council (CSC) under contract No. 201708080130.

References

Al-Dirawi and Bayly, A.E.: A new model for the bouncing regime boundary in binary droplet collisions. Physics of Fluids, Vol. 31, 027105 (2019)

Chen, R.-H. and Chen, C.-T.: Collision between immiscible drops with large surface tension difference: diesel oil and water. Experiments in Fluids, Vol. 41, 453 – 461 (2006)

Chen, R.-H., Wang, W.-C. and Chen, Y.-W.: Like-drop collisions of biodiesel and emulsion diesel. European Journal of Mechanics B/Fluids, Vol. 60, 62 – 69 (2016)

Dukowicz, J.K.: A particle-fluid numerical model for liquid sprays. J. of Computational Physics, Vol. 35, 229 – 253 (1980)

Estrade, J.-P., Carentz, H., Lavergne, G., Biscos, Y.: Experimental investigation of dynamic binary collision of ethanol droplets - a model for droplet coalescence and bouncing. International Journal of Heat and Fluid Flow, Vol. 20, 486 – 491 (1999)

Finotello, G., Kooiman, R.F., Padding, J.T., Buist, K.A., Jongsma, A., Innings, F. and Kuipers, J.A.M.: The dynamics of milk droplet-droplet collisions. Experiments in Fluids, Vol. 59, 17 (2018 a)

Finotello, G., De, S., Vrouwenvelder, J.C.R., Padding, J.T., Buist, K.A., Jongma, A., Innings, F., Kuipers, J.A.M.: Experimental investigation of non-Newtonian droplet collisions: the role of extensional viscosity. Experiments in Fluids, Vol. 59, 113 (2018 b)

Ho, C.A. and Sommerfeld, M.: Modelling of micro-particle agglomeration in turbulent flow. Chem. Eng. Sci., Vol. 57, 3073 – 3084 (2002)

Hu, C., Xia, S., Li, C., Wu, G.: Three-dimensional numerical investigation and modeling of binary alumina droplet collisions. International Journal of Heat and Mass Transfer 113, 569 – 588 (2017)

Huang, K.L. and Pan, K.L.: Size effect on the transition from coalescence to bouncing regime in binary droplet collision. ICLASS 2015, 13th Triennial International Conference on Liquid Atomization and Spray Systems, Tainan, Taiwan, August 23-27, 2015

Kuschel, M. and Sommerfeld, M.: Investigation of droplet collisions for solutions with different solids content. Experiments in Fluids, Vol. 54, 1440 (2013)

Lain, S. and Sommerfeld, M.: Influence of droplet collision modelling in Euler/Lagrange calculations of spray evolution. International Journal Multiphase Flow, Vol. 132, 103392 (2020)

O´Rourke P.J.: Collective drop effects on vaporizing liquid sprays. *Dissertation*, Los Alamos National Laboratory, New Mexico (1981)

Pan, K.-L., Tseng, Y.-H., Chen, J.-C., Huang, K.-L., Wang, C.-H. and Lai, M.-C.: Controlling droplet bouncing and coalescence with surfactants. J. Fluid Mech. Vol. 799, 603 – 636 (2016)

Perini, F. and Reitz, R.D.: Improved atomization, collision and sub-grid scale momentum coupling models for transient vaporizing engine sprays. Int. J. Multiphase Flow, Vol. 79, 107 – 123 (2016)

Pischke, P., Kneer, R. and Schmidt, D.P.: A comparative validation of concepts for collision algorithms for stochastic particle tracking. Computers & Fluids, Vol. 113, 77 – 86 (2015)

Qian, J. and Law, C.K.: Regimes of coalescence and separation in droplet collision. Journal of Fluid Mechanics, Vol. 331, 59 – 80 (1997)

Rüger, M., Hohmann, S., Sommerfeld, M. and Kohnen, G. Euler/Lagrange calculations of turbulent sprays: The effect of droplet collisions and coalescence. Atomization and Sprays, Vol. 10, 47 – 81 (2000)

Sommerfeld, M. and Lain, S.: From elementary processes to the numerical prediction of industrial particle-laden flows. Multiphase Science and Technology, Vol. 21, 123 – 140 (2009)

Sommerfeld, M. and Kuschel, M.: Modelling droplet collision outcomes for different substances and viscosities. Experiments in Fluids, Vol. 57, 187 (2016)

Sommerfeld, M. and Lain, S.: Numerical analysis of sprays with an advanced collision model. ILASS–Europe 2017, 28th Conference on Liquid Atomization and Spray Systems, 6 – 8 September 2017, Valencia, Spain, pp. 418 – 431 (2017)

Sommerfeld, M.: Numerical methods for dispersed multiphase flows. In: Particles in Flows (Eds. T. Bodnár, G.P. Galdi, Š. Neččasová), Series Advances in Mathematical Fluid Mechanics, Springer International Publishing, 327 – 396 (2017)

Sommerfeld, M. and Pasternak, L.: Advances in Modelling of Binary Droplet Collision Outcomes: A review of available results. International Journal of Multiphase Flow, Vol. 117, 182 – 205 (2019)

Sui, M., Sommerfeld, M. and Pasternak, L.: Modelling the occurrence of bouncing in droplet collision for different liquids. ILASS–Europe 2019, 29th Conference on Liquid Atomization and Spray Systems, 2-4 September 2019, Paris, France (2019)

Zhang, J., Mi, J. and Wang, H.: A new mesh-independent model for droplet/particle collision. Aerosol Science and Technology, Vol. 46, 622 – 630 (2012)